Length-scale distribution functions and conditional means for various fields in turbulence

LIPO WANG AND NORBERT PETERS

Institut für Technische Verbrennung, RWTH-Aachen, Templergraben 64, Aachen, Germany

Dissipation elements are identified for various direct numerical simulation (DNS) fields of homogeneous shear turbulence. The fields are those of the fluctuations of a passive scalar, of the three components of velocity and vorticity, of the second invariant of the velocity gradient tensor, turbulent kinetic energy and viscous dissipation. In each of these fields trajectories starting from every grid point are calculated in the direction of ascending and descending gradients, reaching a local maximum and minimum point, respectively. Dissipation elements are defined as spatial regions containing all the grid points from which the same pair of minimum and maximum points is reached. They are parameterized by the linear length between these points and the difference of the field variable at these points.

In analysing the changes that occur during one time step in the linear length as well as in the number of grid points contained in the elements, it is found that rapid splitting and attachment processes occur between elements. These processes are much more frequent than the previously identified processes of cutting and reconnection. The model for the length-scale distribution function that had previously been proposed is modified to include these additional processes. Comparisons of the length-scale distribution function for the various fields with the proposed model show satisfactory agreement.

The conditional mean difference of the field variable at the minimum and maximum points of dissipation elements is calculated for the passive scalar field and the three components of velocity. While the conditional mean difference follows the 1/3 inertial-range Kolmogorov scaling for the passive scalar field, the scaling exponent differs from the 1/3 law for each of the three components of velocity. This is thought to be due to the relatively high shear rate of the DNS calculations.

The conditional mean viscous dissipation shows, differently from all other field variables analysed, a pronounced dependence on the linear length of elements. This is explained by intermittency. This finding is used to evaluate the production and the dissipation term of the empirically derived ε-equation that is often used in engineering calculations.

1. Introduction

The concept of an energy cascade introduced by Richardson (1922) implies that there is a sequence of geometric objects of decreasing size in a turbulent flow over which the kinetic energy 'cascades' until it finally is dissipated by viscous effects. Kolmogorov (1941a, b) made this concept quantitative by rewriting the von-Kármám–Howarth equation, see von Kármán & Howard (1938), for the two-point correlation

function of velocity fluctuations in terms of structure functions, and by using order-of-magnitude and dimensional scaling arguments. Deviations from Kolmogorov's scaling laws, for instance in terms of higher moments of velocity differences, have been the subject of extensive research ever since. Reviews are given by Sreenivasan & Antonia (1997) and Frisch (1995).

> Although much valuable insight has been obtained by studying structure functions, it has become increasingly clear that a deeper understanding of turbulence requires more information about the spatial organization of the underlying flow than two-point measurements can provide. In fact 'the structure function' tells us virtually nothing about the structure of turbulent fluctuations if the latter term is interpreted in the geometrical sense . . . .

This quotation from Chertkov & Pumir (2000), where the authors advocate a four-point approach, illustrates the discontent of many researchers with the present understanding of the statistical geometry of turbulence (see also Tsinober 2001). The question that we therefore have posed (Wang & Peters 2006; Peters & Wang 2006) is whether the flow itself exhibits its structure via well-defined points. We believe that such points are local minimum and maximum points of a fluctuating field, where the field variable may be a passive scalar such as temperature, a component of the velocity vector, a component of the vorticity vector, or the second invariant of the velocity gradient tensor. The field variable may even be the kinetic energy or its dissipation since these quantities are of particular interest in turbulence modelling.

In the previous papers, inspired by the analysis of zero-gradient points by Gibson (1968), we have analysed the fields of the fluctuating passive scalar obtained from direct numerical simulations (DNS) by gradient trajectories that started from each grid point in the direction of ascending and descending scalar gradients. These trajectories invariably end at local maximum and minimum points, respectively, if the scalar field satisfies the conditions for a Morse function. This is a sufficiently smooth function which can be approximated by a pure quadratic form in the vicinity of its extremal points. Since the scalars mentioned above are smoothed by viscosity or by diffusivity, this assumption is likely to be valid. For this reason the method cannot be used for the pressure field, since this field is not diffusive and does not behave like a Morse function in the vicinity of extremal points. Once a local minimum and a local maximum point have been associated with each grid point via the trajectories, finite spatial regions called dissipation elements can be identified. They cover the ensemble of grid points from which the same pair of minimum and maximum points have been reached. These regions are quite irregular in shape and in some cases not even simply connected. Nevertheless, differently from vortex tubes, which often are viewed as geometrical objects representing turbulence, they are space-filling and unambiguously defined by the gradient trajectory algorithm.

This method also provides two parameters that we believe to be the first choice to parameterize the geometry and the field variable structure of the elements: the linear distance between the extremal points and the absolute value of the difference of the field variable at these points. There may be a need to introduce more parameters to characterize the shape of the elements (see Bermejo-Moreno & Pullin 2008) and the distribution of the field variable within them as research along these lines proceeds. On average, however, the elements appear to be elongated structures with a mean length of the order of the Taylor scale (see Wang & Peters 2006).

The distribution of the length of the elements, represented by the linear distance between the extremal points, was the main subject of Wang & Peters (2006) for the passive scalar field. It will be the focus of this paper for the other field variables

listed above. In addition, certain mean quantities, conditioned on the linear length of elements, will be examined, because they are thought to be of fundamental interest for the understanding of turbulence.

Such a quantity is the conditional mean dissipation $\langle \varepsilon | l \rangle$ defined as a volume average for elements of length l:

$$\langle \varepsilon | l \rangle = \frac{\sum_i^{n_l} \int_{V_{i,l}} \varepsilon(\boldsymbol{x}, t) \, \mathrm{d}V_{i,l}}{V_f(l)} = \frac{\int_{V_f} \varepsilon(\boldsymbol{x}, t) \, \mathrm{d}V_f(l)}{V_f(l)}, \tag{1.1}$$

where n_l is the number of elements in a unit volume having linear length in the range $l - \Delta l/2 \leqslant l \leqslant l + \Delta l/2$, $V_{i,l}$ is their individual volume, and the fractional volume within the unit volume occupied by all of them is $V_f(l) = \sum_i^{n_l} V_{i,l}$. This may be used to define $V_l = V_f(l)/n_l$ as the mean volume of elements of length l and $A_l = V_l/l$ as the corresponding mean cross-sectional area. In the previous paper it was shown that, while the length of elements varies, the mean cross-sectional area A_l is approximately constant, of the order of the Kolmogorov scale, and Reynolds number independent. Similarly to (1.1), the overall mean value of ε may be calculated from

$$\langle \varepsilon(t) \rangle = \frac{\int_0^\infty \int_{V_f} \varepsilon(\boldsymbol{x}, t) \, \mathrm{d}V_f(l) \, \mathrm{d}l}{V}, \tag{1.2}$$

where V is the unit volume and the integration over l replaces the summation over fractional volumes. If the length-scale distribution $P(l, t)$, which is proportional to n_l, is known, the overall mean can then be calculated using (1.1) and (1.2) as

$$\langle \varepsilon(t) \rangle = \frac{\int_0^\infty \langle \varepsilon | l \rangle \, V_l P(l, t) \, \mathrm{d}l}{\int_0^\infty V_l P(l, t) \, \mathrm{d}l} \approx \frac{\int_0^\infty \langle \varepsilon | l \rangle \, l P(l, t) \, \mathrm{d}l}{\int_0^\infty l P(l, t) \, \mathrm{d}l}, \tag{1.3}$$

assuming A_l as constant. Since we will derive a model equation for $P(l, t)$ for the various fields we will be able to address certain unresolved fundamental questions regarding the modelling of the ε-equation often used in engineering applications.

We will modify the Boltzmann-type equation, often referred to as a population balance equation, for $P(l, t)$ that had been derived in Wang & Peters (2006) for the scalar field, to include the influence of conditional strain that had previously been neglected. We will also review the mechanisms of generation and removal of elements. We will analyse the DNS data with respect to the rapid changes of elements that we observe during a very small time step. It appears that rapid splitting and attachment of elements are the dominating processes.

The paper is organized as follows: In the next section we will visualize dissipation elements at two consecutive times in the numerical simulations and describe the rapid changes that occur. In §3 we will derive a modified model equation for the length-scale distribution function and compare its steady-state solution with those obtained from DNS of the various fields mentioned above. In §4 we consider conditional means of the difference at the minimum and maximum points for the field variables of the passive scalar field and the fields of the three velocity components. Finally in §5 we will present unexpected observations concerning the conditional mean dissipation rate and draw conclusions for the modelling of the ε-equation.

Case	1	2	3
Number of grid cells	512^3	512^3	1024^3
Viscosity ν	0.01	0.003	0.002
r.m.s. velocity v_{rms}	2.02	1.32	1.38
Turbulent kinetic energy k	6.13	2.61	2.85
Dissipation ε	2.592	0.974	0.939
Taylor scale λ	0.488	0.284	0.246
$Re_\lambda = v_{rms}\lambda/\nu$	98.7	125.0	170.0
Kolmogorov scale η	0.0249	0.0129	0.0096
Resolution $\Delta x/\eta$	0.493	0.95	0.638
Normalized velocity gradient Sk/ε	3.54	4.018	4.554
Scalar variance $\langle \phi'^2 \rangle$	0.0616	0.0287	0.0331
Scalar dissipation $\langle \chi \rangle$	0.0544	0.0245	0.0236

TABLE 1. Non-dimensional mean quantities characterizing three cases considered.

Case 1

	ϕ'	v_1'	v_2'	v_3'	ω_1	ω_2	ω_3	Q	k	ε
l_m	0.947	0.995	0.901	0.858	0.604	0.566	0.564	0.471	0.779	0.413
Extr. points	3014	1351	1536	1757	5953	6912	7521	10533	3374	18837
Elements	9673	5214	5836	6903	23202	27581	29120	41811	12547	74977

Case 2

l_m	0.476	0.534	0.502	0.503	0.290	0.285	0.285	0.243	0.432	0.212
Extr. points	23712	9204	9771	10230	61307	60114	61205	78930	18066	147804
Elements	85868	40177	42843	45169	259913	249527	251544	332897	76933	615802

Case 3

l_m	0.3344	0.4039	0.3763	0.4058	0.1878	0.1863	0.2248	0.1630	0.3357	0.1502
Extr. points	69648	24609	26857	20238	293700	293700	121668	310636	41333	467649
Elements	270180	109752	118926	85224	1271669	1278075	515523	1367515	172319	2025325

TABLE 2. Mean length scales l_m, number of extremal points and number of dissipation elements obtained for the various fields in the three DNS cases.

2. Splitting and attachment of dissipation elements

We have performed three DNS within a cubic box of 2π side length for homogeneous incompressible turbulent shear flow with an imposed velocity gradient $S = d\langle v_1 \rangle/dx_2 = 1.5$. These calculations were continued from the first two cases reported in Wang & Peters (2006) with 512^3 grid points in cases 1 and 2 and with 1024^3 grid cells in case 3. In addition the field of the passive scalar ϕ with unity Prandtl number with an imposed scalar gradient $S_\phi = d\langle \phi \rangle/dx_2 = 1/(2\pi)$ was calculated. The three cases, listed in table 1, differ by the choice of the viscosity ν and consequently the Taylor-scale Reynolds number. In each case the ratio of the grid size Δx to the Kolmogorov scale η is less than unity. This was found to be necessary for grid independence in terms of the number of extremal points and the number of elements. Those numbers are given for the various fields in table 2.

The numerical method used was a spectral collocation method described in some detail in Wang & Peters (2006). From the Fourier coefficients not only the values of the independent variable of the fields mentioned above but also its derivatives in

the three spatial directions were calculated. In order to identify minima and maxima points we calculated trajectories starting from every grid point in the direction of ascending and descending scalar gradients.

The distribution of minimum and maximum points in the cubic box was shown previously in Wang & Peters (2006). In order to illustrate the size of elements and their dynamics we show in figure 1 for the passive scalar field of case 1 two projections of half of the cubic box towards one side plane at two consecutive time steps. For each dissipation element the (blue) minimum point and the (red) maximum point are connected by a straight yellow line. At the centre point of that line a light blue sphere is shown, the volume of which corresponds to the number of grid points of the dissipation element. It is seen that there are many small elements and only a few large elements in the box. While the location of many of the extremal points is nearly the same for the two consecutive snapshots, some of the connecting lines have switched and, more predominantly in this illustration, the size of the spheres has changed. There are also new extremal points that have appeared and others that have disappeared.

These changes cannot be interpreted by the model that we have formulated in the previous paper (Wang & Peters 2006), where a linear array of dissipation elements connected at their end points was considered. The length-scale distribution function in this model resulted from the cutting (and thereby removal) of larger elements to generate smaller elements and from the reconnection by diffusion (thereby generating larger elements and removing smaller elements). We see by comparing the two plots of figure 1 that at many locations there also appears to be a splitting of elements, illustrated by a decrease of the size of a sphere.

On the other hand, there are also increases of the sizes of some of the spheres, indicating attachment of previously split elements having the same length. There also can be generic attachments, like the reverse process of saddle line splitting, which will be discussed below.

An example illustrating the cutting of a larger element into three pieces (where the intermediate piece was assumed to disappear rapidly in the previous linear model) is shown in figure 2. This type of change is a rare event and difficult to identify among the many elements that fill up the box. The original element in (*a*) extends between the red maximum point at the top and the blue minimum point at the bottom. There is a pronounced saddle line in the light green region. The cutting occurs below this region in such a way that the lower part of the elements connects with a new maximum point to which a third element is also connected (the three new elements are shown at a small separation distance from each other). While the structure of the upper new element corresponds to that of the original element, there is a change of shape in the lower and the third element in (*a*).

More common is the splitting of an element into two smaller ones as shown in figure 3. This element, like the one in figure 2, is obtained from the field of the passive scalar. The original element is shown in (*a*) together with a vortex tube in grey that touches it on the top. The shape of the vortex tube was obtained by visualizing contour surfaces of the second invariant of the velocity gradient tensor $Q = \omega^2 - S_{ij}S_{ij}$. The gradient trajectories run between the red maximum point at the top and the blue minimum point towards the right of the element. The splitting occurs in the region, where the vortex tube touches the element. The resulting two elements are shown in figure 3(*b*). While the volumes of the resulting two elements differ considerably they have nearly the same linear length and scalar difference.
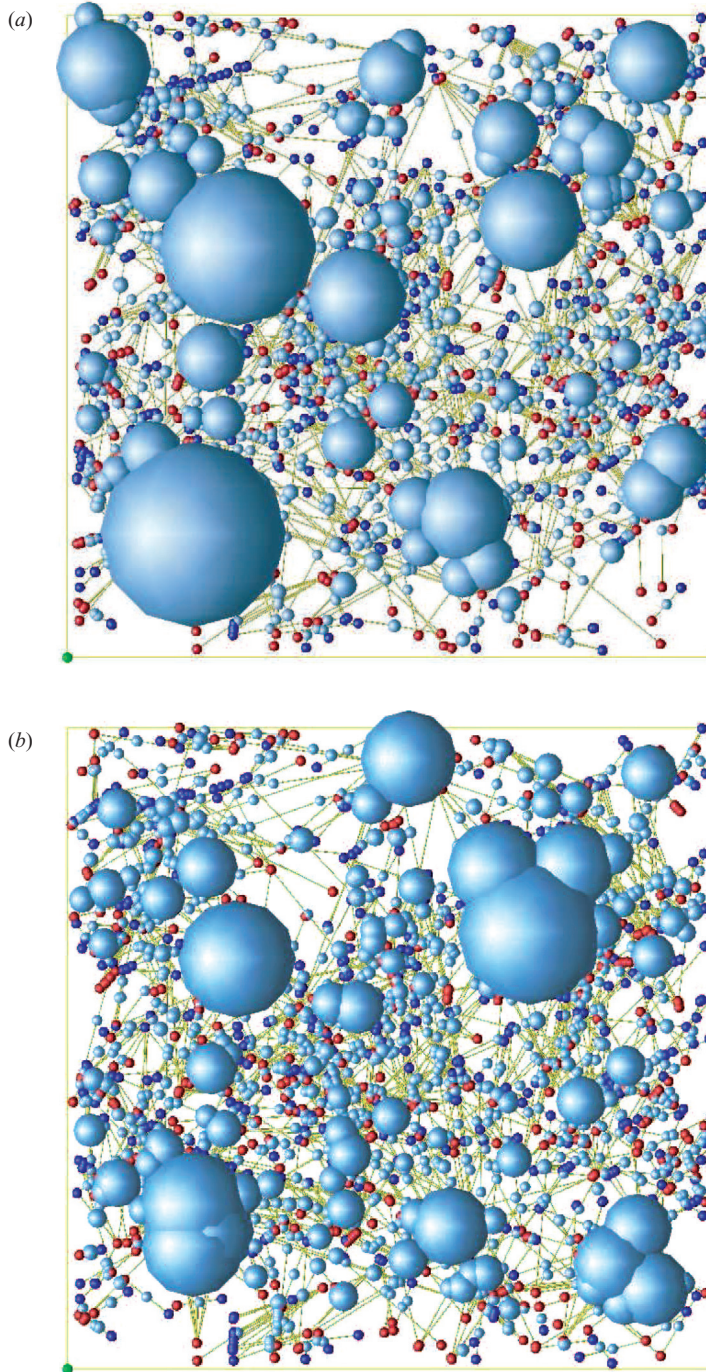
FIGURE 1. Two projections of dissipation elements from half of the cubic box. They are 0.001 time units apart, where 0.08 time units correspond to one Kolmogorov time. Dissipation elements are presented by a light blue sphere on a yellow straight line which connects its (blue) minimum point with its (red) maximum point. Differences in the size of the spheres and the location of extremal points illustrate the rapid changes that occur even during a small fraction of the Kolmogorov time.
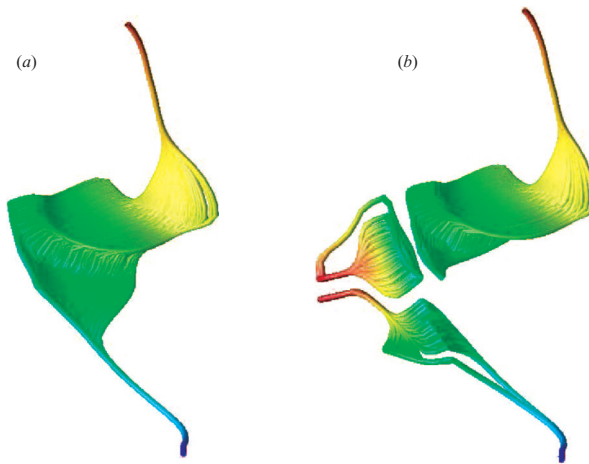
FIGURE 2. An example of the cutting of a dissipation element (*a*) from the passive scalar field into three pieces (*b*). The shapes of dissipation elements are illustrated by showing the trajectories between the minimum and the maximum point. The colour coding which ranged from blue for the minimum to red for the maximum in (*a*) was maintained after cutting.
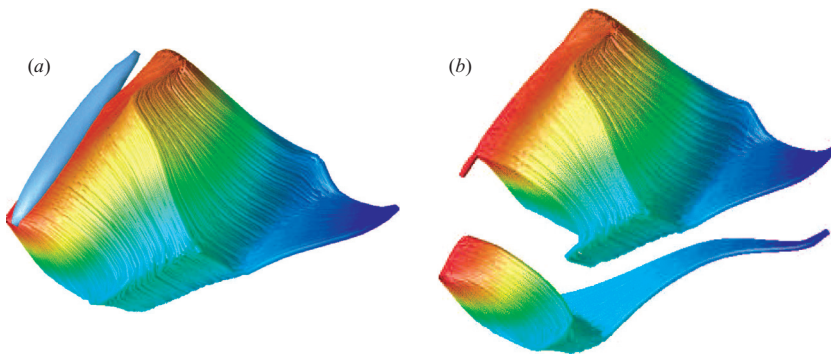
FIGURE 3. An example of splitting of a dissipation element from the passive scalar field into two pieces. The splitting is initiated by a region of strong vorticity shown in (*a*).
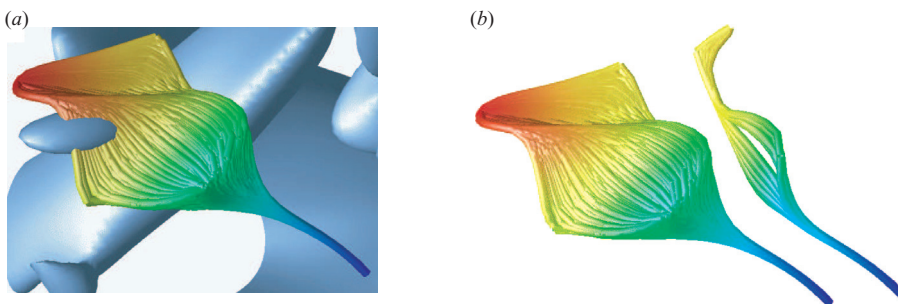
FIGURE 4. An example of splitting of a dissipation element from the v_1-velocity field. A smaller element is split off by the action of vorticity shown in (*a*).

The splitting of an element taken from the field of the v_1-velocity component is shown in figure 4. It is surrounded by several regions of strong vorticity as shown in (*a*). The interaction with the turbulent motion leads to the split-off of a thin element that has a smaller linear distance and a scalar difference from the original element.

Figure 5 shows an element taken from the field of the second invariant of the velocity gradient tensor. The interaction of the element with a vortex tube shown in (*a*) hides the region of maximum Q (in red) as it should, since when the vorticity is large Q should be large. The splitting off of a smaller element shown in (*b*) apparently originates from this region.

Figure 6 shows two different elements taken from the field of the kinetic energy k. The element in (*a*) is sheet-like and wraps around a vortex tube. The element in (*b*) is more voluminous but shows that regions of large vorticity are spatially separated from those of large kinetic energy. This behaviour was found in all simultaneous visualizations of elements from the kinetic energy field with vortex tubes. One may easily demonstrate that this should be so by analysing periodic arrays of counter-rotating vortices of opposite vorticity at the same magnitude. There, the maximum of kinetic energy lies half-way between two vortices, whereas the maximum of absolute vorticity lies at the centre of the vortices.

Finally, figure 7 shows the splitting of an element taken from the field of the viscous dissipation ε. Here a vortex tube just touches the original element in (*a*) which then splits into two elements of nearly equal linear length and scalar difference in (*b*).

While all the examples in figures 3, 4, 5, and 7 show splitting processes, we were unsuccessful in identifying attachment processes, which would have required analysing fields at three different consecutive times. That such processes must also occur can be inferred from the arguments given above. Such an attachment of two elements would be the inverse of the splitting process and can be imagined as a time reversal of the processes shown in figures 3, 4, 5 and 7. Physically, this must involve the disappearance of newly generated extremal points by the combined action of random motion and molecular diffusion.

3. Modelling

In Wang & Peters (2006) we considered a birth-and-death process for a class of elements of length l in order to derive an equation for the probability density $P(l, t)$ (or distribution function) of l. We have shown that, at least on average, the elements are elongated structures with diameter of a few Kolmogorov scales and therefore considered a one-dimensional model of linearly connected rod-like elements which were cut into smaller elements by a random Poisson process. When a very small element disappears due to diffusion the two adjacent elements reconnect to a larger element. In a following paper (Peters & Wang 2006), by considering a random superposition of Gaussian profiles in one dimension as a model problem, we showed that not all cuttings were successful and that the frequency of the random cutting process must scale with the integral time scale. Since the integral time and the molecular diffusivity are the only input parameters in the three-dimensional DNS, dimensional analysis then shows that, with molecular diffusion coefficient $D = \nu$, the mean length scale of the three-dimensional DNS data is of the order of the Taylor scale, rather than any other length scale in the problem.
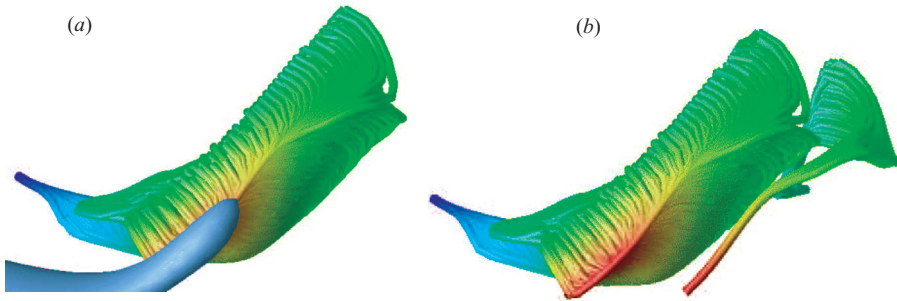
(a) (b)

FIGURE 5. An example of splitting of a dissipation element from the field of the second invariant Q. A region of high vorticity covers the (red) maximum point in (a). The off-splitting seems to originate from this region.
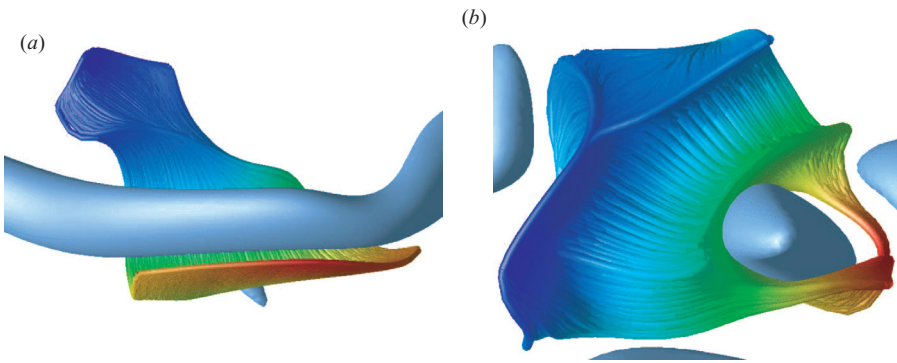
(b)

(a)

FIGURE 6. Two different elements from the field of kinetic energyshowing the interaction with regions of strong vorticity.
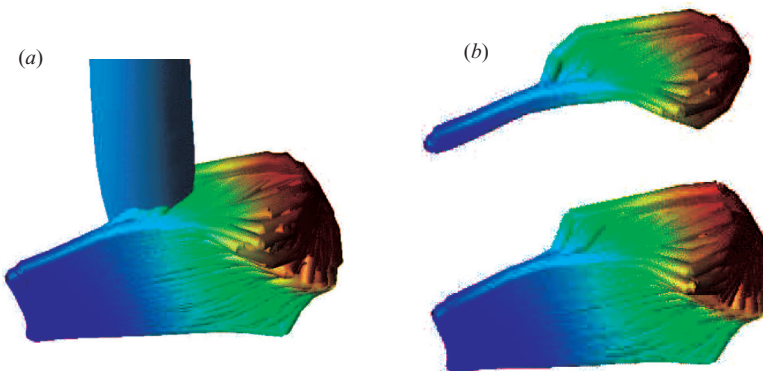
(a) (b)

FIGURE 7. An example of splitting of an element from the field of viscous dissipation.

Summarizing the results of both papers, the equation for the normalized probability density $\tilde{P}(\tilde{x}, \tilde{t})$ is

$$\frac{\partial \tilde{P}(\tilde{x}, \tilde{t})}{\partial \tilde{t}} + \frac{\partial [\tilde{v}_D(\tilde{x}) \tilde{P}(\tilde{x}, \tilde{t})]}{\partial \tilde{x}} = \Lambda \left[2 \int_{\tilde{x}}^{\infty} \tilde{P}(\tilde{x}, \tilde{t}) \, \mathrm{d}y - \tilde{x} \, \tilde{P}(\tilde{x}, \tilde{t}) \right]$$

$$+ 8 \left. \frac{\partial \tilde{P}(\tilde{x}, \tilde{t})}{\partial \tilde{x}} \right|_{\tilde{x} \to 0} \left[\int_0^{\tilde{x}} \frac{\tilde{y}}{\tilde{x}} \tilde{P}(\tilde{x} - \tilde{y}, \tilde{t}) \tilde{P}(\tilde{y}, \tilde{t}) \, \mathrm{d}\tilde{y} - \tilde{P}(\tilde{x}, \tilde{t}) \right]. \quad (3.1)$$

Here the independent variable x representing a class of length l was non-dimensionalized as $\tilde{x} = \rho x$, where ρ is the inverse of the mean length scale l_m:

$$\rho = \frac{1}{l_m}. \quad (3.2)$$

Likewise y, representing the class from which reconnection occurs, was non-dimensionalized as $\tilde{y} = \rho y$ and $P(x, t)$ was non-dimensionalized as $\tilde{P}(\tilde{x}, \tilde{t}) = P(x, t)/\rho$. Finally, the time t and the drift velocity v were non-dimensionalized as $\tilde{t} = t \rho^2 D$ and $\tilde{v}_D = v_D/(\rho D)$. In (3.1) the strain term accounting for the axial compression of elements appearing in Wang & Peters (2006) is no longer considered.

In Peters & Wang (2006) it was shown that the drift velocity $v_D(x)$ obtained from the linear model problem may be approximated well by the ansatz

$$v_D(x) = -\frac{4D}{x} (1 - c\rho x \, \exp(-\rho x)), \quad (3.3)$$

where the constant c was determined from the condition that the total length L of the linear array must not change:

$$\int_0^{\infty} v_D(x) P(x, t) \, \mathrm{d}x = 0. \quad (3.4)$$

For convenience and comparison with the previous model we will use the same ansatz here.[†] The other model used in Wang & Peters (2006) also was tested. It was found that the differences in the resulting probability density were negligible. This is mainly due to the constraint imposed by (3.4).

It is worth mentioning that (3.1) is parameter free since the Péclet number Λ was determined as

$$\Lambda = \frac{\lambda}{\rho^3 D} \quad (3.5)$$

from the normalization condition

$$\int_0^{\infty} \tilde{P}(\tilde{x}, \tilde{t}) \, \mathrm{d}\tilde{x} = 1. \quad (3.6)$$

Furthermore, since the mean length scale was used for normalization, the following condition for the first moment also must be satisfied:

$$\int_0^{\infty} \tilde{x} \, \tilde{P}(\tilde{x}, \tilde{t}) \, \mathrm{d}\tilde{x} = 1. \quad (3.7)$$

[†] In (3.3), differently from Wang & Peters (2006), there is a factor 4 in front of the diffusion coefficient. This factor leads to the factor 8 in the second term on the right-hand side of (3.1) and increases the Péclet number accordingly, but cancels out in the calculation of the normalized probability density.

In the following we will add terms to the equation to account for the additional processes of splitting and attachment. The splitting process will generate shorter elements without altering the length of those from which they have split. We will call this is generation by splitting (gs). The attachment process will remove elements of all classes without generating longer elements. This will be called removal by attachment (ra). Together with the previously (Wang & Peters 2006) identified processes of generation by cutting (gc), removal by cutting (rc), generation by reconnection (gr) and removal by reconnection (rr) we now would have six processes in the birth and death of elements. However, because the cutting and reconnection processes occur very rarely, we will neglect them at the end.

We will again consider the transition of n_l grid cells within a class of elements of length l. Denoting the number density of elements per unit volume by N, the number of grid cells per unit volume within a class of elements of length l is $n_l N P(l, t) \, dl$. The time rate of change of the number of grid cells leaving and entering class x of elements is

$$\frac{\partial}{\partial t} [n_x N P_x(x, t)] \, dx = \int W(x|y) \, n_y \, N P_y(y, t) \, dy \, dx - \int W(y|x) \, n_x \, N P_x(x, t) \, dy \, dx. \tag{3.8}$$

Here we have denoted by x the class of elements under consideration, while y stands for the class of elements from which transitions to x occurs. Furthermore, $W(x|y)$ and $W(y|x)$ are the transition probabilities per unit time from y to x and from x to y, respectively. Differently from Wang & Peters (2006) and Peters & Wang (2006) we have included the number density N in all terms. This will become of interest when unsteady changes of $P(x, t)$ are considered in future work.

After division by dx (3.1) now has six terms on the right-hand side:

$$\frac{\partial}{\partial t} [n_x N P_x] = \frac{\partial}{\partial t} [n_x N P_x]_{\text{gc}} + \frac{\partial}{\partial t} [n_x N P_x]_{\text{rc}} + \frac{\partial}{\partial t} [n_x N P_x]_{\text{gr}}$$
$$+ \frac{\partial}{\partial t} [n_x N P_x]_{\text{rr}} + \frac{\partial}{\partial t} [n_x N P_x]_{\text{gs}} + \frac{\partial}{\partial t} [n_x N P_x]_{\text{ra}}. \tag{3.9}$$

The first four of these have been derived in Wang & Peters (2006). The generation-by-splitting term

$$\frac{\partial}{\partial t} [n_x N P_x]_{\text{gs}} = \int_x^\infty W_{\text{gs}}(x|y) \, n_y \, P_y(y, t) \, dy \tag{3.10}$$

represents the generation of typically smaller elements by the splitting process from larger elements. The integration runs from $y = x$ to infinity because the newly generated element of length x is assumed to be smaller than or equal to the element of length y from which it splits.

The process is similar to the generation by cutting (gc). The transition probability density per unit time $W_{\text{gs}}(x|y)$ is again proportional to a rate ω times the probability density $P_{x \to y}(x, y, t)$ that such splitting generates elements of class x:

$$W_{\text{gs}}(x|y) = \omega \, P_{x \to y}(x, y, t). \tag{3.11}$$

However, the rate ω of secondary splitting is not only proportional to the length y of the element that is cut, as in the model of linearly connected rod-like elements, but also proportional to the surface of elements, since splitting can occur at any part of the surface. Therefore we write $\omega(y)$ as

$$\omega(y) = \lambda_s \, y^2, \tag{3.12}$$

where λ_s is a splitting frequency per unit time and area which needs to be determined from the normalization condition. It implicitly contains a factor which accounts for the average number of elements generated by the splitting. Assuming $P_{y \to x}$ to be the same as in Wang & Peters (2006), namely

$$P_{y \to x} = 2 \frac{x}{y^2}, \qquad (3.13)$$

the integral on the right-hand side of (3.10) will become

$$\frac{\partial}{\partial t} [n_x \, N P_x]_{\mathrm{gs}} = 2 \, \lambda_s \int_x^\infty x \, n_y \, N P_y(y, t) \, \mathrm{d} y. \qquad (3.14)$$

Next we will consider the removal of elements by attachment (ra):

$$\frac{\partial}{\partial t} [n_x \, N P_x]_{\mathrm{ra}} = - n_x \, N P_x \int_0^\infty W_{\mathrm{ra}}(y \,|\, x) \, \mathrm{d} y. \qquad (3.15)$$

This process describes the attachment of two or more elements to larger ones due to the disappearance of extremal points. The integration here runs from $y = 0$ to $y = x$ because all element classes may be removed. The transition probability density per unit time $W_{\mathrm{ra}}(y \,|\, x)$ of this removal process is proportional to the rate $\omega(x)$. We assume that this rate is proportional to the length of the circumference of the element which again is proportional to the element length x. The frequency per unit time and length is denoted by μ_a, such that $W_{\mathrm{ra}}(y \,|\, x) = \mu_a \, x \, P_{x \to y}$. Since elements of class x under consideration are removed by any class y, the corresponding probability density of transitions $P_{x \to y}$ will be independent of y and uniform in $0 \leqslant y \leqslant x$ with the normalization condition

$$\int_0^x P_{x \to y} \, \mathrm{d} y = 1. \qquad (3.16)$$

Therefore the integral describing the removal of elements by attachment becomes

$$\frac{\partial}{\partial x} [n_x \, N P_x]_{\mathrm{ra}} = \mu_a \, n_x \, N \, x \, P(x, t). \qquad (3.17)$$

Based on the rod-line nature of the elements we will assume as in Wang & Peters (2006) that the number n_x (or n_y) of grid points is proportional to the length x (or y) of an element.

Dividing (3.8) by n_x and the number density N, one therefore obtains, with the formulation of the (gc), (rc), (gr) and (rr) processes taken from Wang & Peters (2006),

$$\frac{1}{N} \frac{\partial}{\partial t} [N P(x, t)] = 2 \, \lambda_s \int_x^\infty y \, P(y, t) \, \mathrm{d} y + 2 \lambda \beta \int_x^\infty P(y, t) \, \mathrm{d} y$$

$$- (\mu_a + \lambda \beta) x \, P(x, t) + 2 \mu \beta \left[\int_o^x \frac{y}{x} P(x - y, t) P(y, t) \, \mathrm{d} y - P(x, t) \right]. \qquad (3.18)$$

In (3.18) we have multiplied the cutting and reconnection terms by a weighting factor β to account for the influence of the terms previously considered. In the following we will only consider the limit $\beta \to 0$ because these processes occur very rarely as noted above.

In addition, we will consider the compression and elongation of elements by the different velocities at the maximum and minimum points. For this purpose we have evaluated the conditional mean velocity difference $\langle \Delta \boldsymbol{v} \cdot \boldsymbol{n} \,|\, l \rangle$, divided by the linear length l, where $\boldsymbol{n}$ is in the direction of the linear length, for the various fields. This
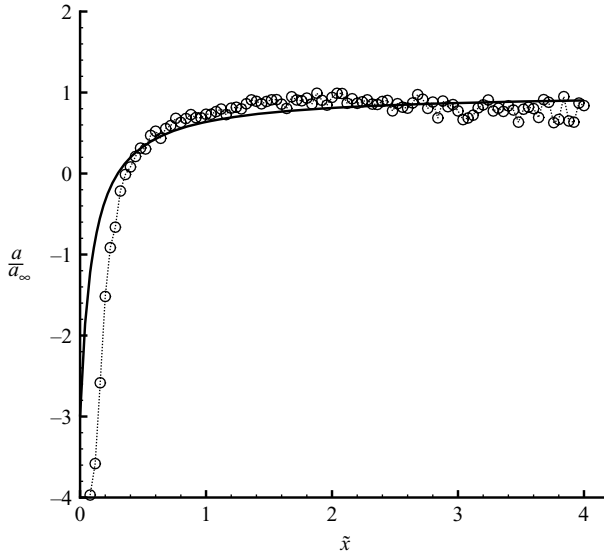
FIGURE 8. Conditional mean strain rate, normalized by its value $a_\infty = 1.85$ at $l \to \infty$ between the minimum and the maximum point of elements obtained from the passive scalar field in case 3. The solid line is the approximation (3.20).

quantity represents the conditional mean strain rate of the element class l

$$a = \frac{\langle \Delta \boldsymbol{v} \cdot \boldsymbol{n} \,|\, l \rangle}{l}. \tag{3.19}$$

It was normalized as $\tilde{a} = a/a_\infty$ using its value a_∞ at $l \to \infty$ and is shown for the passive scalar field in figure 8 as a function of $\tilde{x} = l/l_m$. It is approximated by

$$\tilde{a} = 1 - \frac{0.4}{\tilde{x} + 0.1}. \tag{3.20}$$

The value of a_∞ must be obtained from the numerical analysis of the various DNS fields. Values of a_∞ for the ε-field, as an example, will be given in table 4 in §5. They are close to the value $S = \mathrm{d}\langle v_1 \rangle / \mathrm{d} x_2 = 1.5$ for three cases presented.

We also need to consider the drift process due to molecular diffusion. The factor $4D$ in (3.3) was derived for the linear model problem and does not take three-dimensional effects with a random geometry of the small elements into account. In order to account for this we will multiply the ansatz (3.3) by an enhancement coefficient c_e. We normalize the time in (3.18) as $\tilde{t} = t a_\infty$, and the velocity in (3.3) as $\tilde{v}_D = v_D/(l_m a_\infty)$ to obtain in the limit $\beta \to 0$ the non-dimensionalized equation for a time-independent number density N:

$$\frac{\partial \tilde{P}(\tilde{x}, \tilde{t})}{\partial \tilde{t}} + \frac{\partial}{\partial \tilde{x}} \left[\tilde{v}_D(\tilde{x}) \, \tilde{P}(\tilde{x}, \tilde{t}) \right] + \frac{\partial}{\partial \tilde{x}} \left[\tilde{a} \tilde{x} \tilde{P}(\tilde{x}, \tilde{t}) \right] = \Lambda_s \int_{\tilde{x}}^{\infty} \tilde{y} \tilde{P}(\tilde{y}, \tilde{t}) \, \mathrm{d}\tilde{y} - \Lambda_a \, \tilde{x} \, \tilde{P}(\tilde{x}, \tilde{t}), \tag{3.21}$$

where $\Lambda_s = 2 \lambda_s / (\rho^2 a_\infty)$ and $\Lambda_a = \mu_a / (\rho a_\infty)$ are non-dimensionalized numbers whose values will be determined from the normalization and the first moment during the solution of the equation. Numerically obtained values are shown in table 3. The

D_e	Λ_s	Λ_a	c
0.6	3.13	3.33	3.90
1.0	3.77	3.66	3.74
1.5	4.41	3.94	3.62

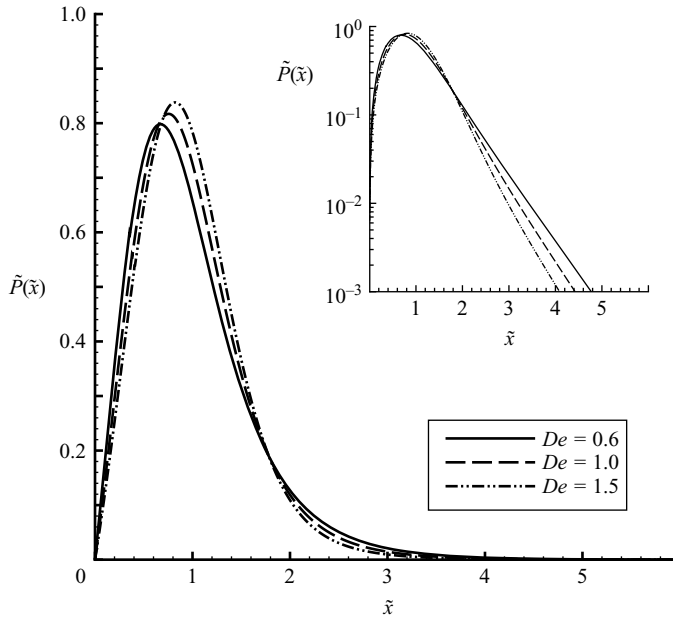TABLE 3. Parameters in (3.21) obtained as eigenvalues of the solution.

FIGURE 9. Distribution function of the linear length of elements for three values of the modelling parameter D_e defined in (3.23) as given in table 3.

non-dimensional drift velocity is

$$\tilde{v}_D = -\frac{D_e}{\tilde{x}} \left(1 - c\,\tilde{x}\exp(-\tilde{x})\right), \tag{3.22}$$

where

$$D_e = 4Dc_e / \left(l_m^2\, a_\infty\right) \tag{3.23}$$

is an effective non-dimensional diffusivity. Since l_m^2 is proportional to the square of the Taylor scale, which itself is proportional to the viscosity ν, the molecular transport coefficients cancel out for $D = \nu$ in this definition. It then follows that the model equation (3.21) is Reynolds number independent.

For three different values of D_e to be used below, the resulting probability densities are shown in figure 9 in a linear plot, with a log-linear plot in the inset. There is a shift of the maximum value to larger $\tilde{x}$ for increasing D_e. The slope of the exponential tail is also reduced.

In order to understand the balance between the different terms in (3.21) we have plotted them for the case $De = 0.6$ as a function of $\tilde{x}$ in figure 10. It is seen that for small $\tilde{x}$ there is a balance between the generation-by-splitting (gs) term and the drift term. This illustrates that small elements generated from large elements by splitting
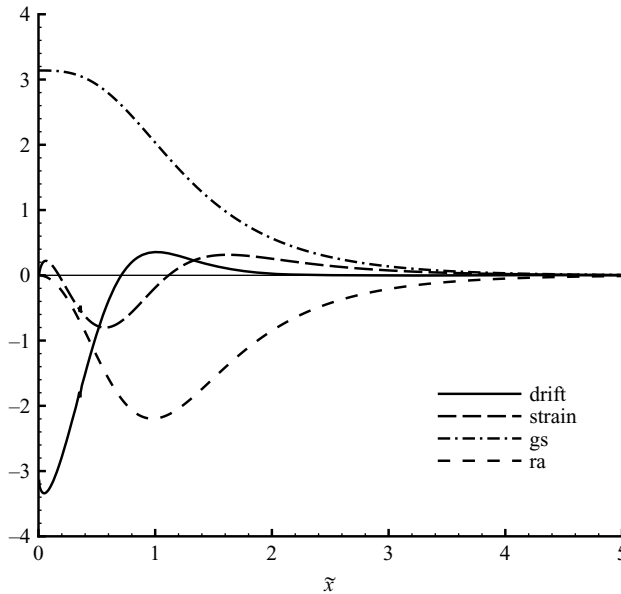
FIGURE 10. Different terms in the steady-state solution of the model equation (3.21) for the length-scale distribution function. To show the balance, the sign of the drift and the strain term has been changed.

eventually disappear due to molecular diffusion. The strain term changes sign twice. The compressive strain close to $\tilde{x} = 0$ generates smaller elements, while the extensive strain generates larger elements for large $\tilde{x}$. Both are removed from an intermediate region where $\tilde{P}(\tilde{x}, \tilde{t})$ has a maximum. Finally, the removal-by-attachment (ra) term balances the other three terms.

The comparison of the model with probability densities calculated for the various fields from the DNS are shown in figures 11–16. Plotted are the three cases for the fluctuating passive scalar field ϕ' (figure 11), the fluctuating velocity components v_1', v_2' and v_3' (figure 12) as well as the components of the vorticity ω_1, ω_2 and ω_3 (figure 13), and the second invariant Q (figure 14), respectively. Also shown are those for the kinetic energy k (figure 15) and its dissipation ε (figure 16). It is seen that for the passive scalar ϕ' the DNS data agree best for $D_e = 0.6$, in particular in the log-linear inset. For all other fields except the velocities v_2' and v_3' the value $D_e = 1$ shows a much better agreement. The difference of DNS data for the probability densities of the v_2' and v_3' fields with that of v_1', for instance, is not large but, nevertheless, a value of $D_e = 1.5$ was chosen to approximate these p.d.f.s. There is little difference between the three DNS cases in each of the plots, not enough to suspect a Reynolds number dependence of the shape of the distributions. This was taken into account in the formulation of the model equation.

4. Conditional mean scalar differences

In this section we explore the scaling laws for the conditional means of the scalar difference between the value at the minimum and the maximum points of the dissipation elements and compare them with those for the structure functions. As shown in Wang & Peters (2006) for the passive scalar field the joint probability density of the linear distance between the minimum and the maximum points and the
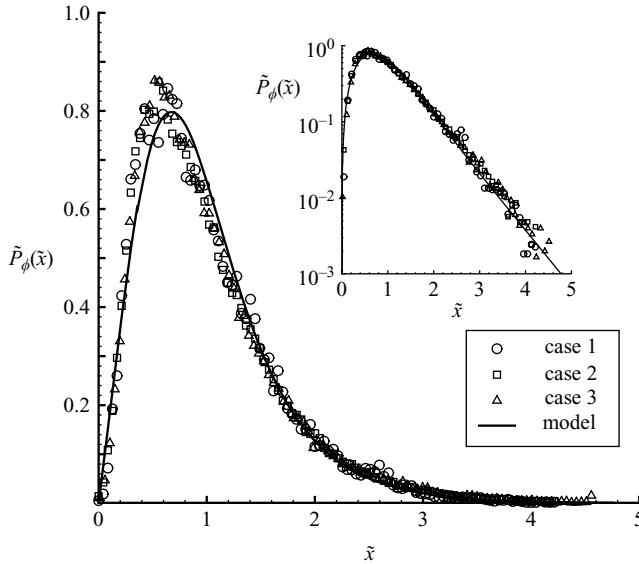
FIGURE 11. Comparison of the length-scale distribution function from the DNS data for the fluctuations of the passive scalar with the present model. $De = 0.6$.

absolute value of the difference of the field variable at these points can be obtained for the various fields considered here. From these the length-scale distribution functions considered above can be determined as marginal probability densities, and also the conditional mean can be evaluated.

In figures 17 and 18 we present compensated plots for the conditional means $\langle \Delta\phi'|l \rangle$, $\langle \Delta v_1'|l \rangle$, $\langle \Delta v_2'|l \rangle$ and $\langle \Delta v_3'|l \rangle$. For the three cases considered. As in Wang & Peters (2006) the mean conditional difference of the passive scalar $\langle \Delta\phi'|l \rangle$ scales in the inertial range for over more than one decade as $1/3$ ($= -(-5/3 + 1)/2$), corresponding to the Kolmogorov $-5/3$ scaling. It starts again at approximately 7η which is much smaller than values quoted in the literature for classical structure functions. This favourable behaviour of dissipation element analysis was explained in Wang & Peters (2006) with the higher two-point correlation in the vicinity of extremal points, which contaminates classical structure function analysis when relatively small Reynolds-number DNS data are used. Dissipation element analysis avoids the high correlation regions in the vicinity of extremal points by construction.

On the other hand, the conditional means of the velocity differences at the minimum and maximum points $\langle \Delta v_1'|l \rangle$, $\langle \Delta v_2'|l \rangle$ and $\langle \Delta v_3'|l \rangle$ (figure 18) do not follow the $1/3$-scaling. Larger deviations from the Kolmogorov scaling exponents for velocity components than for the scalar were also reported by Mydlarski (2003) for quasi-isotropic grid turbulence. For the present shear flow situation, the imposed strain rate $S = \partial\langle v_1 \rangle/\partial x_2$ appears to be too large for the assumption of isotropic turbulence to be valid (S. Sarkar 2006, personal communication). In figure 19 we plot the conditional mean difference of the v_1'-velocity component divided by l, $\langle \Delta v_1'|l \rangle/l$, over $\tilde{x}$. This quantity differs fundamentally from the conditional mean strain rate defined in (3.19), which was the velocity difference in the direction of the linear length. When compared with the imposed mean strain rate $S = \partial\langle v_1 \rangle/\partial x_2 = 1.5$, it is seen that for large $\tilde{x}$ this quantity is only a factor 2 larger than the imposed strain rate. Another criterion for isotropic turbulence was put forward by Saddoughi & Veeravalli (1994). It states that
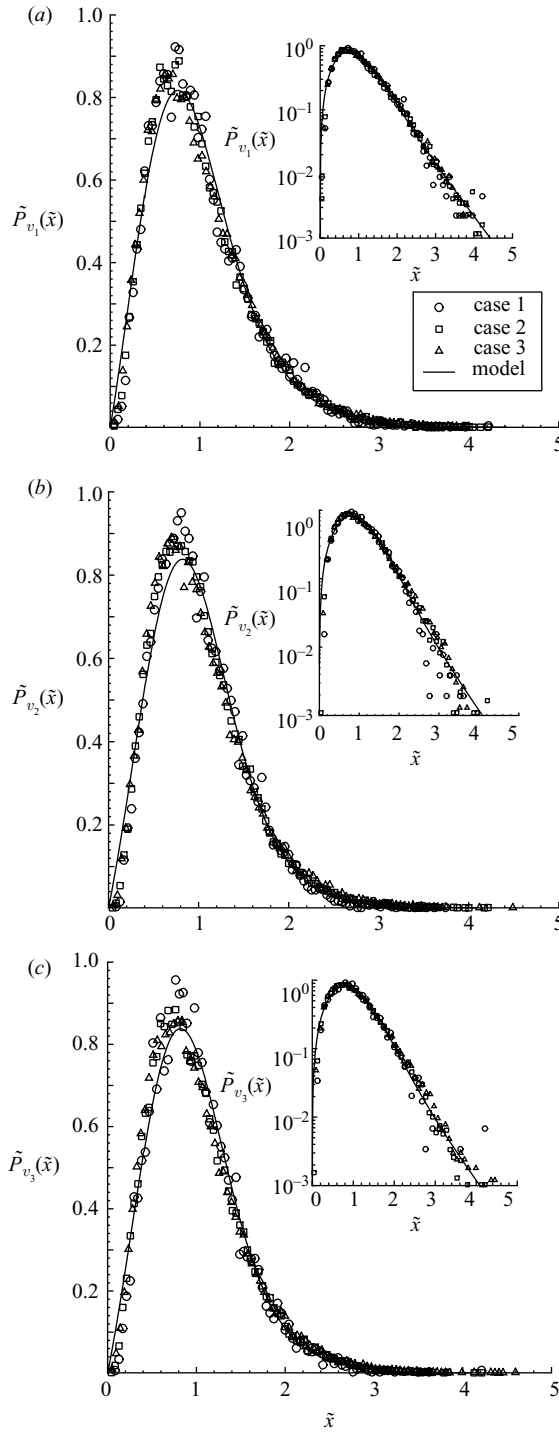
FIGURE 12. Comparison of the length-scale distibution function from the DNS data for the fluctuation of (*a*) the v_1-velocity field (*b*) the v_2-velocity field and (*c*) the v_3-velocity field, with the present model for $D_e = 1.0$, 1.5, 1.5 respectively.
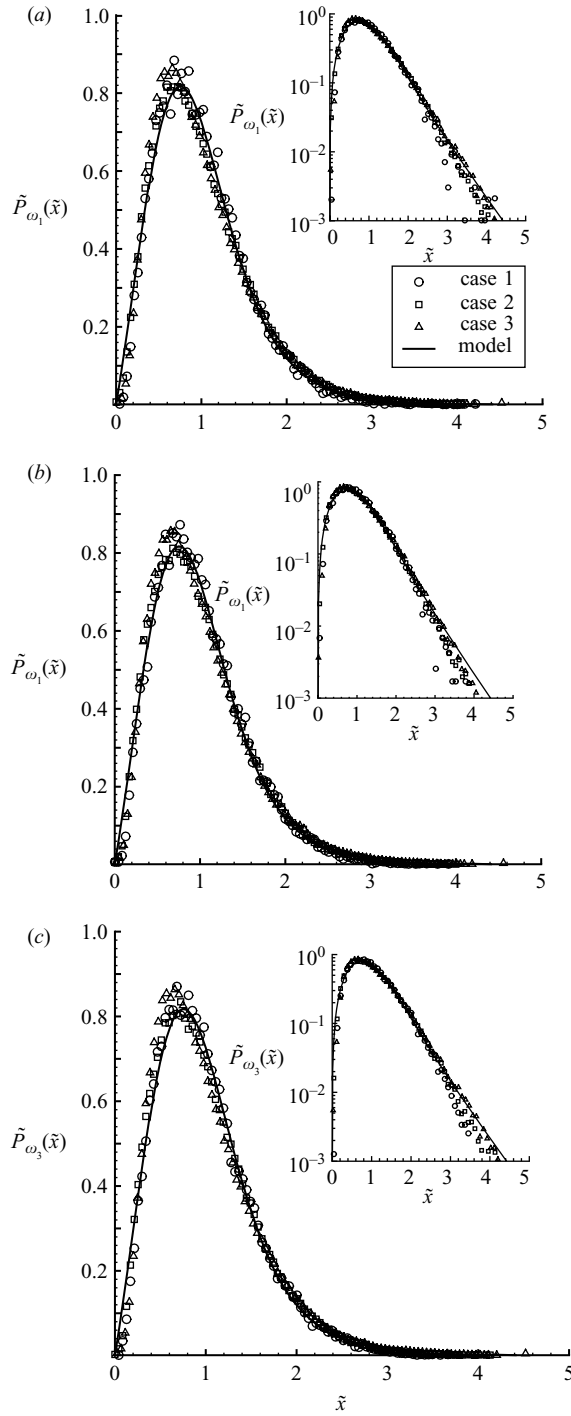
FIGURE 13. As figure 12 but for (*a*) the ω_1-vorticity field, (*b*) the ω_2-vorticity field and (*c*) the ω_3-vorticity field, with the present model for $D_e = 1.0$.
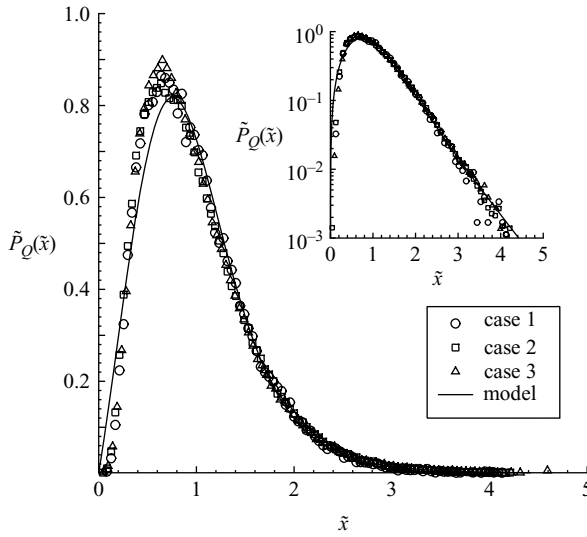
FIGURE 14. As figure 12 but for the second invariant of the velocity gradient tensor Q for $D_e = 1.0$.
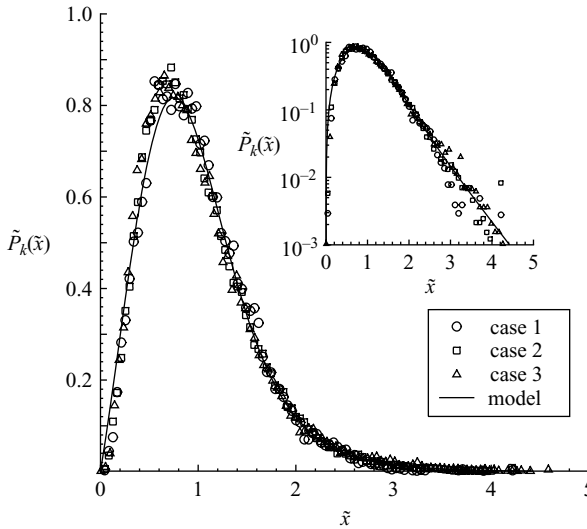
FIGURE 15. As figure 12 but for the turbulent kinetic energy k for $D_e = 1.0$.

the product $S(\nu/\varepsilon)^{1/2}$ should not be more than about 0.01, whereas it is 0.03 for case 1, 0.083 for case 2 and 0.069 for case 3 in our computation.

5. The special case of the conditional dissipation rate

In view of the particular importance of dissipation in turbulence we explore how it is distributed over the different classes of dissipation elements. We have calculated
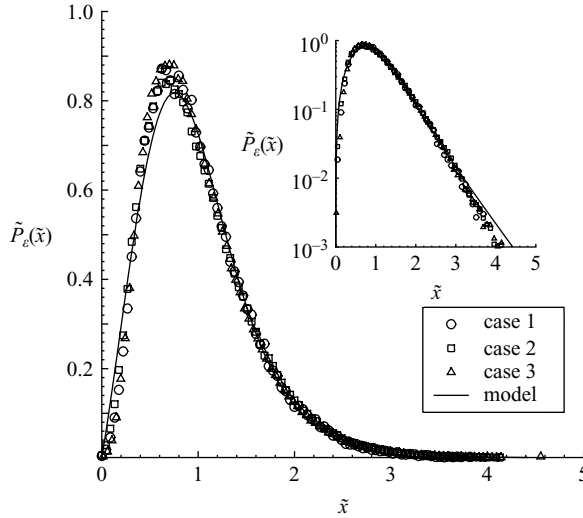
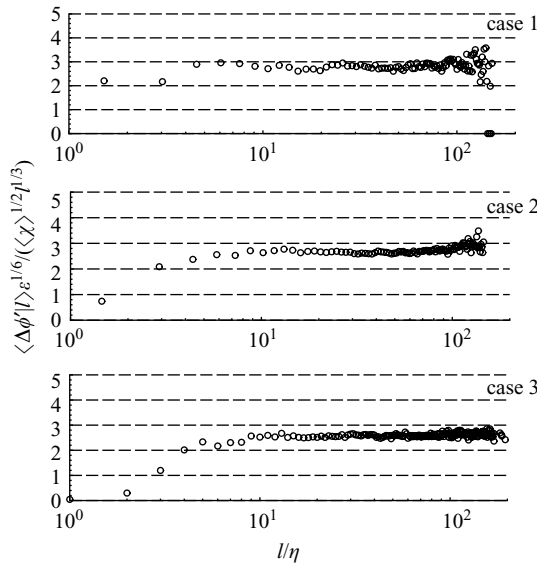FIGURE 16. As figure 12 but for the viscous dissipation ε for $De = 1.0$.

FIGURE 17. Compensated conditional mean difference of the fluctuating passive scalar at the minimum and the maximum points of dissipation elements. The exponent of $1/3$ for l in all cases corresponds to Kolmogorov's inertial image scaling.

the conditional mean $\langle \varepsilon | l \rangle$ for each class $\tilde{x}$ of length scales taken from the ε-field for the three cases considered. Here ε was weighted by the number of grid points in the dissipation element. These results are plotted in a log-log plot in figure 20 showing that the conditional mean decreases. This may be explained by the intermittent nature of dissipation. In figure 21 we show the local dissipation from case 2 taken along a line within the box. Even at this relatively low Reynolds number we observe intermittency, characterized by very high local peaks together with regions of very low activity. Dissipation elements calculated from the ε-field would extend between a
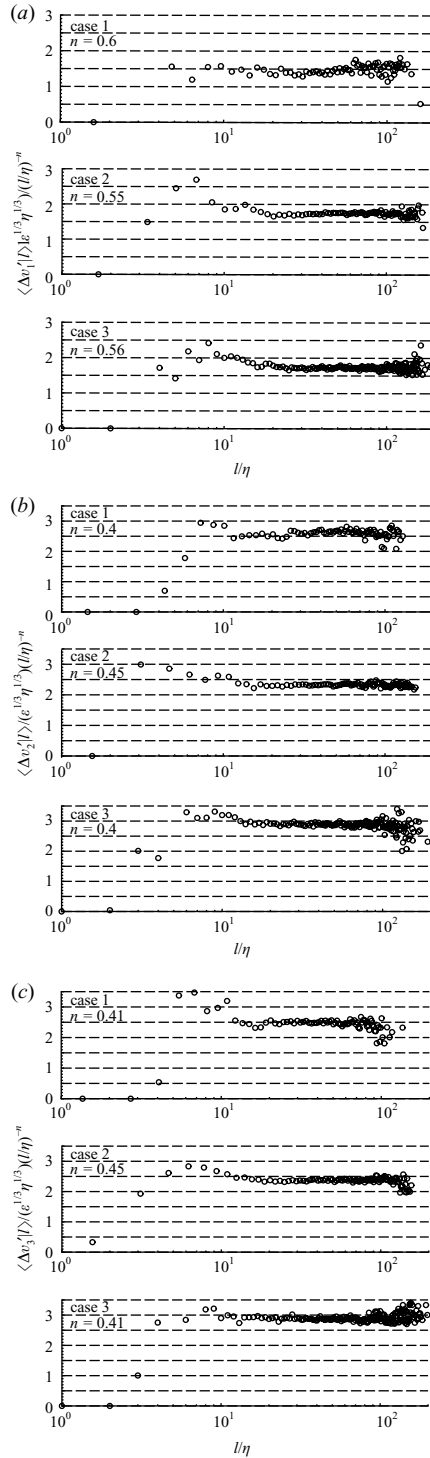
FIGURE 18. Compensated conditional mean difference of (*a*) the fluctuating v_1-velocity, (*b*) the fluctuating v_2-velocity and (*c*) the fluctuating v_3-velocity at the maximum and minimum points of dissipation elements. The exponents n for l/η used in the compensation differ from the expected Kolmogorov scaling.
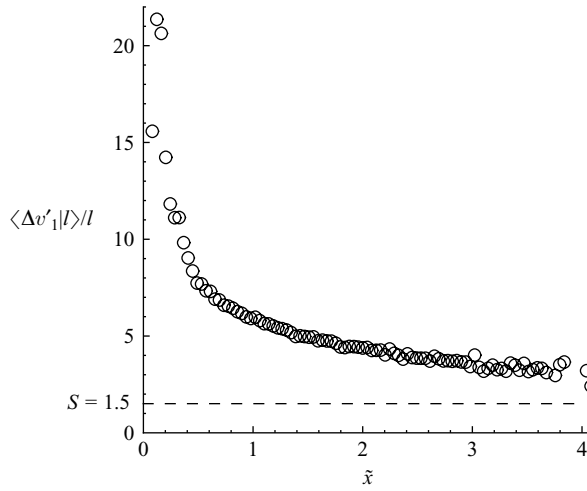
FIGURE 19. Conditional mean strain rate $\langle \Delta v'_1 | l \rangle / l$ calculated from case 2 in figure 18(a) compared with the imposed mean strain rate $S = \partial \langle v_1 \rangle / dx_2$.
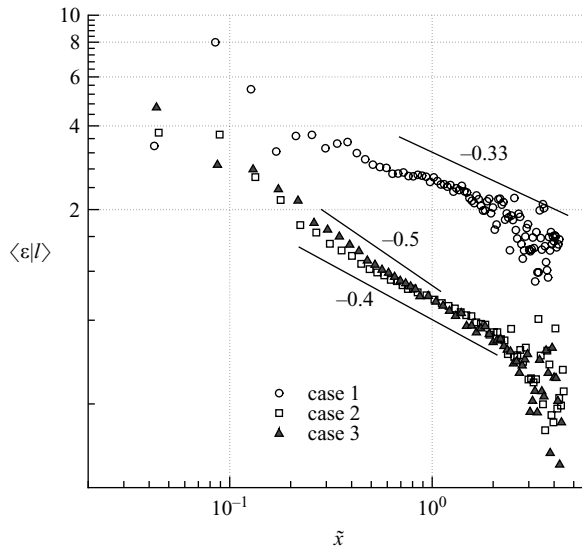

FIGURE 20. Conditional mean dissipation $\langle \varepsilon / l \rangle$ within elements.

local maximum point on a peak and a minimum in the low-activity region. Elements having a large linear length naturally will contain a larger portion of the low-activity region where ε is low. Therefore the mean value of ε for large elements is smaller than for small elements.

Ever since Obukhov's and Kolmogorov's third hypothesis (Obukhov 1962; kolmogorov 1962) the intermittency of ε has been viewed as the key to the understanding of the fine-scale structure of turbulence. Meneveau & Sreenivasan (1991) as well as Frisch (1995) have provided multifractal analyses which shed new light on the early log-normal model for $\varepsilon(r)$. In that model there is no length-scale dependence of the mean dissipation but there is one for the variance. The length scale r in the log-normal model corresponds to the radius of the sphere over which the dissipation
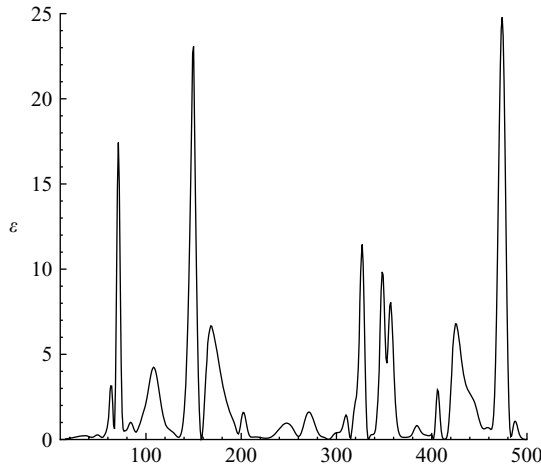
FIGURE 21. Dissipation along a line within the box illustrating intermittency.
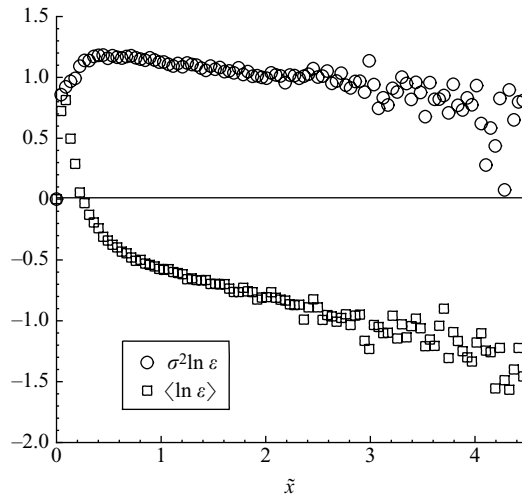

FIGURE 22. Mean and variance of $\log \varepsilon$ as a function of the normalized length of elements for case 2.

is averaged (see Pope 2000, p. 259). This differs from the present definition of a length scale determined from dissipation elements which is not independent of the ε-field itself. Figure 22 shows that if we take the log of ε and determine its variance $\sigma_{\ln \varepsilon}^2$ as a function of the element class, it turns out to be nearly independent of the length scale, while the mean of $\log \varepsilon$ decreases as the mean itself. The exponent in figure 20 varies for the three cases shown which suggests a Reynolds number dependence of this exponent at the relatively small Reynolds numbers of the simulation.

Conditional means of all the other non-intermittent fields which fluctuate between positive and negative values were found to be zero as expected. The conditional mean turbulent kinetic energy, calculated from its field, is found to have positive slope of 0.1 for case 1, of 0.05 for case 2 and is almost constant and equal to its overall mean for case 3.

We will use the finding for $\langle \varepsilon | l \rangle$ to shed some light on the form of the ε-equation often used in engineering models, and its empirical coefficients. For the present case of homogeneous shear flow this equation is

$$\frac{\mathrm{d}\langle \varepsilon \rangle}{\mathrm{d}t} = c_{\varepsilon 1} \langle -v_1' v_2' \rangle \frac{\langle \varepsilon \rangle}{\langle k \rangle} \frac{\mathrm{d}\langle v_1 \rangle}{\mathrm{d}x_2} - c_{\varepsilon 2} \frac{\langle \varepsilon \rangle^2}{\langle k \rangle}, \tag{5.1}$$

where the coefficients are typically chosen as $c_{\varepsilon 1} = 1.44$ and $c_{\varepsilon 2} = 1.9$. Approximating the conditional mean dissipation by

$$\langle \varepsilon | l \rangle = \varepsilon^* \tilde{x}^{-n} \tag{5.2}$$

and using the definition of $\langle \varepsilon \rangle$ given in (1.3) one obtains

$$\langle \varepsilon \rangle = \varepsilon^* \int_0^\infty (\tilde{x})^{1-n} \tilde{P}(\tilde{x}, \tilde{t}) \, \mathrm{d}\tilde{x}. \tag{5.3}$$

In order to evaluate the production and dissipation terms in the ε-equation we multiply both sides of the non-dimensional model equation (3.21) by $\varepsilon^* \tilde{x}^{1-n}$ and integrate. Then we obtain for the derivative with respect to the dimensional time t

$$\frac{\partial \langle \varepsilon \rangle}{\partial t} = a_\infty \varepsilon^* (I_s - I_a + I_{\text{strain}} + I_{\text{drift}}), \tag{5.4}$$

where the integrals result from the respective terms in (3.21).

We will associate the drift term, which is the only one to contain the molecular diffusivity, with the dissipation term in the ε-equation. Consequently, the splitting and attachment terms which model the rapid changes due to turbulent motion and the strain term should sum to the production term. Since (3.21) was evaluated for the steady-state case the sum of these three terms must be equal to the drift term

$$I_s - I_a + I_{\text{strain}} = -I_{\text{drift}}. \tag{5.5}$$

Therefore, in order to calculate both the production term and the dissipation term in (5.1) we need only evaluate the drift integral

$$I_{\text{drift}} = D_e \int_0^\infty \tilde{x}^{1-n} \frac{\partial}{\partial \tilde{x}} \left(\frac{1}{\tilde{x}} (1 - c \tilde{x} \exp(-\tilde{x})) \tilde{P}(\tilde{x}, \tilde{t}) \right) \mathrm{d}\tilde{x}. \tag{5.6}$$

The production term in (5.1) then is equal to $a_\infty \varepsilon^* I_{\text{drift}}$. Equation (5.6) was evaluated with the value $D_e = 1.0$ used for the ε-field for the three different cases. The numbers are given in table 3. Likewise the value a_∞, which was numerically evaluated for the ε-field, and the ratio $\varepsilon^*/\langle \varepsilon \rangle$, equal to the inverse of the integral in (5.3), are shown in that table. By using the empirical relation $\langle -v_1' v_2' \rangle = 0.3 \langle k \rangle$, valid for shear flow (Bradshaw, Ferris & Atwell 1967), we may write the coefficient $c_{\varepsilon 1}$ as

$$c_{\varepsilon 1} = \frac{\varepsilon^*}{\langle \varepsilon \rangle} \frac{a_\infty}{\mathrm{d}\langle v_1 \rangle / \mathrm{d}x_2} \frac{(-I_{\text{drift}})}{0.3}. \tag{5.7}$$

From table 4 it is seen that the values of $c_{\varepsilon 1}$ slowly increase with increasing Reynolds number towards the empirical value $c_{\varepsilon 1} = 1.44$.

In a similar way we may evaluate the coefficient $c_{\varepsilon 2}$ in the dissipation term in (5.1) which also is equal to $a_\infty \varepsilon^* I_{\text{drift}}$. Here we need to relate the mean length l_m of the ε-field given in table 2 to the Taylor scale λ as $l_m = \alpha \lambda$, where λ^2 can be written as

$$\lambda^2 = 10D \frac{\langle k \rangle}{\langle \varepsilon \rangle}, \tag{5.8}$$

	case 1	case 2	case 3	Empirical value
Re_λ	98.7	125.0	170.0	–
n	0.33	0.4	0.5	–
I_{drift}	−0.23	−0.30	−0.40	–
a_∞	0.8	1.1	1.3	–
$\varepsilon^*/\langle\varepsilon\rangle$	1.04	1.04	1.04	–
c_e	3.42	4.12	3.67	–
α^2	0.716	0.557	0.372	–
$c_{\varepsilon 1}$	0.425	0.763	1.20	1.44
$c_{\varepsilon 2}$	0.457	0.923	1.64	1.90

TABLE 4. Numbers needed for the evaluation of the coefficients in the ε-equation.

since $\nu = D$ in the calculation. The diffusivity in the definition of D_e then cancels and the coefficient $c_{\varepsilon 2}$ becomes

$$c_{\varepsilon 2} = 0.4 \, \frac{c_e}{\alpha^2} \, \frac{\varepsilon^*}{\langle\varepsilon\rangle} \, \frac{(-I_{\mathrm{drift}})}{D_e}, \tag{5.9}$$

where (3.23) has been used to evaluate the enhancement coefficient c_e. With the values for α^2 obtained from table 1 and table 2 one may then calculate the coefficient $c_{\varepsilon 2}$ for the three cases. Again, these values increase with increasing Reynolds numbers towards the empirical value $c_{\varepsilon 2} = 1.9$.

We may conclude that the proportionality between l_m and λ and the Reynolds number independence of the model equation (3.21) translate into the form of the empirically derived ε-equation. The coefficients $c_{\varepsilon 1}$ and $c_{\varepsilon 2}$, however, show a Reynolds number dependence.

6. Summary

We have shown that the concept of dissipation elements, previously demonstrated for passive scalars only, can be extended to many other fields in turbulence. The length-scale distribution functions obtained from the DNS then show a similar shape. They were modelled by an equation that contains a single free parameter, D_e, which is used as a modelling constant accounting for differences in the various fields. In the modelling different processes were assumed to be active, namely drift due to diffusion and strain as continuous processes, and splitting and attachment as rapid Poisson-like processes. There seems to be no Reynolds number dependence of the distribution functions but there is for the conditional dissipation rate. This finding is exploited to analyse the modelling assumptions of the empirically derived ε-equation.

There also is a difference between the scalar and the velocity fields in the scaling exponents of the conditional mean differences. It is argued that this is due to the imposed shear and that the velocity field is not really isotropic.

REFERENCES

BERMEJO-MORENO, I. & PULLIN, D. I. 2008 On the non-local geometry of turbulence. *J. Fluid Mech.* **603**, 101–135.

BRADSHAW, P., FERRIS, D. H. & ATWELL, N. P. 1967 Calculation of boundary-layer development using the turbulent energy equation. *J. Fluid Mech.* **28**, 593–616.

CHERTKOV, M. & PUMIR, I. S. 2000 Statistical geometry and Lagrangian dynamics in turbulence. In *Itermittency in Turbulent Flows* (ed. J. C. Vassilicos), pp. 243–261. Cambridge University Press.

FRISCH, U. 1995 *Turbulence: The Legacy of A.N. Kolmogorov*. Cambridge University Press.

GIBSON, C. H. 1968 Fine structure of scalar fields mixed by turbulence I. Zero gradient points and minimal gradient surfaces. *Phys. Fluids* **11**, 2305–2315.

VON KÁRMÁN, T. & HOWARD, L. 1938 On the statistical theory of isotropic turbulence. *Proc. R. Soc. Lond.* **164**, 192–215.

KOLMOGOROV, A. N. 1941*a* Dissipation of energy under locally isotropic turbulence. *Dokl. Akad. Nauk SSSR* **32**, 16–18.

KOLMOGOROV, A. N. 1941*b* The local structure of turbulence in an incompressible viscous fluid for very large Reynolds numbers. *Dokl. Akad. Nauk SSSR* **30**, 301–305.

KOLMOGOROV, A. N. 1962 A refinement of previous hypotheses concerning the local structure of turbulence in a viscous incompressible fluid at high Reynolds number. *J. Fluid Mech.* **13**, 82–85.

MENEVEAU, C. & SREENIVASAN, K. R. 1991 The multifractional nature of turbulent energy dissipation. *J. Fluid Mech.* **224**, 429–484.

MYDLARSKI, L. 2003 Mixed velocity-passive scalar statistics in high-Reynolds-number turbulence. *J. Fluid Mech.* **475**, 173–203.

OBUKHOV, A. R.1962 Some specific features of atmospheric turbulence. *J. Fluid Mech.* **13**, 77–81.

PETERS, N. & WANG, L. 2006 Dissipation element analysis of scalar fields in turbulence. *C. R. Mech.* **334**, 433–506.

POPE, S. 2000 *Turbulent Flows*. Cambridge University Press.

RICHARDSON, L. 1922 *Weather Prediction by Numerical Process*. Cambridge University Press.

SADDOUGHI, S. G. & VEERAVALLI, S. V. 1994 Local isotropy in turbulent boundary layers at high Reynolds number. *J. Fluid Mech.* **268**, 333–372.

SREENIVASAN, K. R. & ANTONIA, R. A. 1997 The phenomenology of small-scale turbulence. *Annu. Rev. Fluid Mech.* **29**, 435–472.

TSINOBER, A. 2001 *An Informal Introduction to Turbulence*. Kluwer.

WANG, L. & PETERS, N. 2006 The length scale distribution function of the distance between extremal points in passive scalar turbulence. *J. Fluid Mech.* **554**, 457–475.